SCIENTIFIC REPORTS

OPEN

Engineering MoS$_x$/Ti/InP Hybrid Photocathode for Improved Solar Hydrogen Production

Qiang Li[1], Maojun Zheng[1,2], Miao Zhong[3], Liguo Ma[1], Faze Wang[1], Li Ma[4] & Wenzhong Shen[1]

Due to its direct band gap of ~1.35 eV, appropriate energy band-edge positions, and low surface-recombination velocity, *p*-type InP has attracted considerable attention as a promising photocathode material for solar hydrogen generation. However, challenges remain with *p*-type InP for achieving high and stable photoelectrochemical (PEC) performances. Here, we demonstrate that surface modifications of InP photocathodes with Ti thin layers and amorphous MoS$_x$ nanoparticles can remarkably improve their PEC performances. A high photocurrent density with an improved PEC onset potential is obtained. Electrochemical impedance analyses reveal that the largely improved PEC performance of MoS$_x$/Ti/InP is attributed to the reduced charge-transfer resistance and the increased band bending at the MoS$_x$/Ti/InP/electrolyte interface. In addition, the MoS$_x$/Ti/InP photocathodes function stably for PEC water reduction under continuous light illumination over 2 h. Our study demonstrates an effective approach to develop high-PEC-performance InP photocathodes towards stable solar hydrogen production.

The imminent depletion of fossil fuels with the increasing environmental concerns has been stimulating considerable research efforts for clean and renewable energy production over the past decades[1–3]. Hydrogen is one of the most promising high-energy-density green fuels. Photoelectrochemical (PEC) water splitting is a highly attractive means to produce hydrogen from water using abundant solar energy[4–6]. Since the pioneering work of hydrogen generation from water splitting using a titanium dioxide (TiO$_2$) electrode[7], enormous efforts have been paid to find suitable semiconductors for efficient PEC hydrogen generation[8–12]. However, the reported solar-to-chemical energy conversion efficiencies are still unsatisfactory. Suitable photoactive semiconductors for efficient solar-driven water splitting must (i) absorb a large portion of light in solar spectrum, (ii) have favorable band edge positions, (iii) possess high stability under PEC operating conditions, (iv) be catalytically active for the hydrogen evolution reaction (HER) or oxygen evolution reaction (OER)[13], and (v) generate a sufficiently high photovoltage. A single semiconductor material is usually difficult to meet all the above requirements and, therefore, effective combination of materials in functional heterogeneous structures or PEC configurations is necessary[14,15]. A common technique is to combine light absorbers with robust water splitting catalysts to enhance photocatalytic activity and stability of the PEC devices.

P-type InP is one of the most promising candidates for PEC hydrogen generation because of its direct band gap of 1.35 eV well-matched to the solar spectrum, favorable conduction band position for hydrogen evolution reaction and low surface-recombination velocity[16]. InP photocathodes have been extensively studied[16–20] and recently reported a high water splitting performance (power-saved efficiency of 15.8%)[21]. However, the practical application of InP in PEC schemes is still limited by the two main drawbacks of (i) the poor stability due to self-photocorrosion in electrolyte solution[22,23]; and (ii) the inefficient surface catalytic activity for hydrogen evolution reactions. Conformal layers of thin TiO$_2$ coatings grown by atomic layer deposition have been wildly employed to stabilize InP[16,21,24,25], and in conjunction with noble metal co-catalysts like Pt[16,21,24] to effect water reduce. Nevertheless, relatively high cost and scarcity of noble metals hindered their large-scale practical applications. Moreover, separated noble metal catalysts on top of InP cannot prevent photocorrosion in InP photocathodes. Although thick layers of noble metals can protect photocathodes, they may also block the underlying InP

[1]Key Laboratory of Artificial Structure and Quantum Control, Ministry of Education, Department of Physics and Astronomy, Shanghai Jiao Tong University, Shanghai, 200240, People's Republic of China. [2]Collaborative Innovation Center of Advanced Microstructures, Nanjing, 210093, People's Republic of China. [3]Department of Chemical System Engineering, The University of Tokyo, 7-3-1 Hongo, Bunkyo-ku, Tokyo 113-8656, Japan. [4]School of Chemistry and Chemical Technology, Shanghai Jiao Tong University, Shanghai, 200240, People's Republic of China. Correspondence and requests for materials should be addressed to M.J.Z. (email: mjzheng@sjtu.edu.cn)
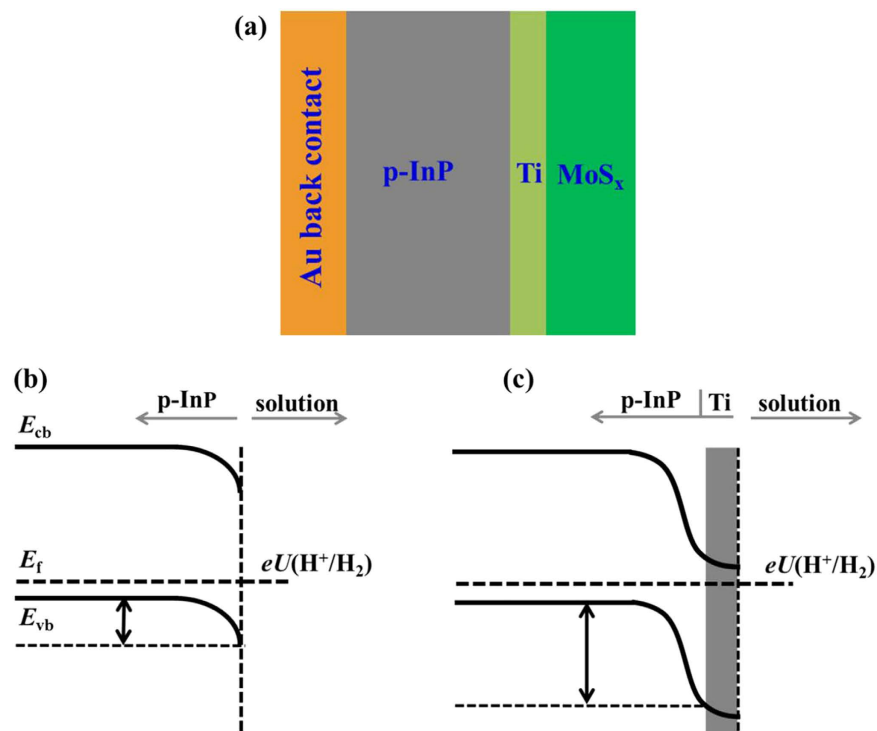
Figure 1. (**a**) Structure of the MoS$_x$ and Ti-coated p-type InP photocathode. (**b,c**) Proposed approximate energy band diagrams of pristine p-InP (**b**) and Ti/p-InP (**c**) photocathodes in equilibrium with the H$_2$/H$^+$ redox couple in water in dark. An enlarged band bending is obtained with the Ti-coated p-InP in electrolyte due to the low work function of Ti metal.

from effectively harvesting light, and decreases the PEC performances. Therefore, low-cost InP-based photocathodes with efficient and stable PEC performances are desirable.

Mo-based chalcogenides have been recently investigated as both a protection layer and an electrocatalyst for hydrogen evolution reaction due to its excellent stability and high electro-catalytic activity[26–30]. Thus, Molybdenum sulfide (MoS$_x$) has a great potential to enhance both stability and activity for InP photocathodes. Indeed, the previous study has shown that the MoS$_3$-modified InP photocathode exhibits a highly stable and large photocurrent density[20]. However, the onset potential was relatively negative in the reported structure likely related to a small photovoltage produced in the InP/electrolyte. The water reduction onset potential of many semiconductors is inherently low, due to the mismatch of the interface energetics between the semiconductor and the electrolyte[21]. To address the intrinsic limitation, several approaches have been used to tune the relative energetics at the semiconductor/electrolyte interface. For instance, an n$^+$ emitter layer can be incorporated on the top surface of p-type semiconductor to form a buried junction between the semiconductor and the electrolyte. This buried junction is expected to produce a high photovoltage by effectively decoupling the band bending in the semiconductor from the semiconductor/liquid contact[26]. Lewis et $al.$ have showed that the HER onset potential could be improved by ~250 mV by using n$^+$ p-Si structure device[31]. In addition to homo-junctions, hetero-junctions with appropriate band positions also function efficiently. A recent work has shown that the introduction of a Ga$_2$O$_3$ buffer layer between the Cu$_2$O and TiO$_2$ can shift the onset potential towards an extremely positive value of 1.02 V vs. RHE[32]. Therefore, a suitable buffer layer is believed to effectively increase the photovoltage by forming a better energy band alignment with the semiconductor.

Herein, we introduce a Ti thin layer as a suitable buffer layer between InP and the MoS$_x$ (denoted as MoS$_x$/Ti/InP) to achieve an improved photovoltage and a stable photocurrent density. The overall material structure is shown in Fig. 1a. The low work function of the Ti layer affords a high Schottky barrier to p-type InP valence band (Fig. 1c). The top MoS$_x$ further acts as an efficient and robust co-catalyst for hydrogen generation. Compared with pristine InP and MoS$_x$/InP, MoS$_x$/Ti/InP exhibits remarkably enhanced PEC performances in terms of onset potentials and photocurrent densities at 0 V vs. RHE. Our study is a first demonstration of MoS$_x$/Ti/InP for efficient and stable PEC water reduction. Such enhancement can be attributed to an improved surface band bending and reduced charge-transfer resistance at the MoS$_x$/Ti/InP/electrolyte interface, proved by Mott-Schottky and electrochemical impedance spectroscopy (EIS) analyses.

Results and Discussion

Figure 2 shows the photoelectrodepositon of amorphous MoS$_x$ (a-MoS$_x$) catalysts on a Ti-coated InP electrode (Ti/InP). The cyclic voltammetry (CV) cycles show clear reduction peaks similar to the previous report from Hu et $al.$[33]. Once the CVs were completed, a uniform catalyst layer on top of the electrode can be clearly seen. The CV cycles for photoelectrodeposition and the precursor concentrations in solution are considered to be
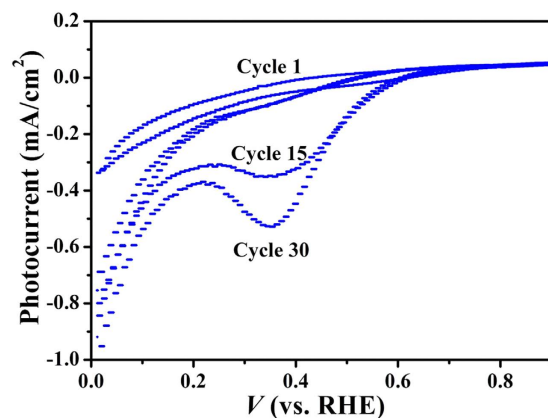
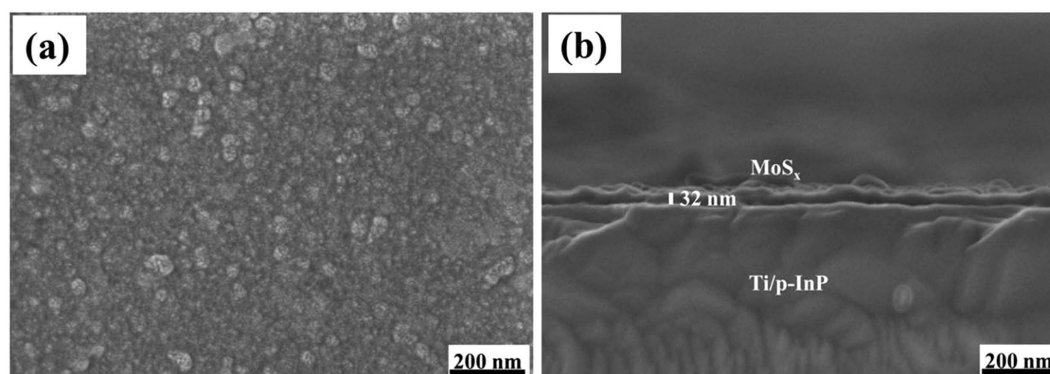**Figure 2. Cyclic voltammetry scans for photoelectrodeposition of MoS$_x$ on Ti-coated p-InP electrodes.**

Figure 3. (**a**) A top-view SEM image of a MoS$_x$/Ti/InP electrode. (**b**) A cross-sectional SEM image of a MoS$_x$/Ti/InP electrode.

important for determining the thickness of a-MoS$_x$ on InP. It is reported that the amount of a-MoS$_x$ on CNTs increases with the increase of deposition cycles or precursor concentrations[34]. The connection between a-MoS$_x$ particles and InP is strong enough against ultra-sonification, which is essential for long-term use for PEC hydrogen production.

The morphology of the deposited a-MoS$_x$ films was examined by scanning electron microscopy (SEM). Figure 3 shows the top view and cross-sectional view SEM images of a ~32 nm thick a-MoS$_x$ film obtained after 30 deposition cycles. The a-MoS$_x$ film (Fig. 3a) consists of nanoparticles assembled in a porous morphology with a high specific surface area, which improves its catalytic activities. Furthermore, the a-MoS$_x$ film uniformly covers the InP surface over a large scale (Fig. 3b). This is also important for protecting InP from oxidation and stabilize it for long time operation.

X-ray photoelectron spectroscopy (XPS) was used to characterize the elemental compositions and their binding energies. The survey scan in Fig. 4a shows that Ti, Mo, and S elements are coexisted in the examined film. The chemical states of Mo and S species in the sample are determined from the high-resolution XPS S 2p and Mo 3d spectra before PEC experiments (Fig. 4b,c). The Mo 3d XPS spectrum features two peaks: Mo 3d$_{5/2}$ at a binding energy of 229.2 eV and Mo 3d$_{3/2}$ at 232.5 eV. These energies are consistent with a +4 oxidation state for Mo as reported previously for MoS$_3$[35,36]. The peak at lower energy position of 226 eV can be ascribed to the S 2s. XPS S 2p spectrum in Fig. 4c exhibits a complex peak, which can be fitted into three featured peaks. The S 2p$_{3/2}$ at 161.9 eV is attributed to terminal S^{2-}, and the S 2p$_{3/2}$ at 163.1 eV can be assigned to bridging S$_2^{2-}$ and/or apical S^{2-} ligands[37–39]. The peak at higher energy (164.5 eV) may be due to residual sulfur from the electrodeposition reactant[37]. Furthermore, quantification analysis by XPS gives a Mo/S ratio of 1:3.4, which is larger than commonly reported for MoS$_x$ ($x \approx 3$). Taken together, the XPS data verifies formation of a-MoS$_x$ phases. It has been reported previously that the abundant exposure of S$_2^{2-}$ in amorphous MoS$_x$ can effectively absorb H with a small free energy, which is advantageous for enhancing the HER activity[40,41]. Therefore, it is believed that InP with abundant active S edge sites should give potentially outstanding HER performances. After the PEC stability experiments, the Mo peaks are shifted toward lower binding energies (Fig. 4d). This shift can be related to a partial reduction of the Mo atoms or to a change in their environment. The intensity of S peak around 161.9 eV is also increased compared to that of the peak at 163.1 eV (Fig. 4e). These results agree with previous reports that amorphous MoS$_2$ might be the most effective water reduction catalyst[33].
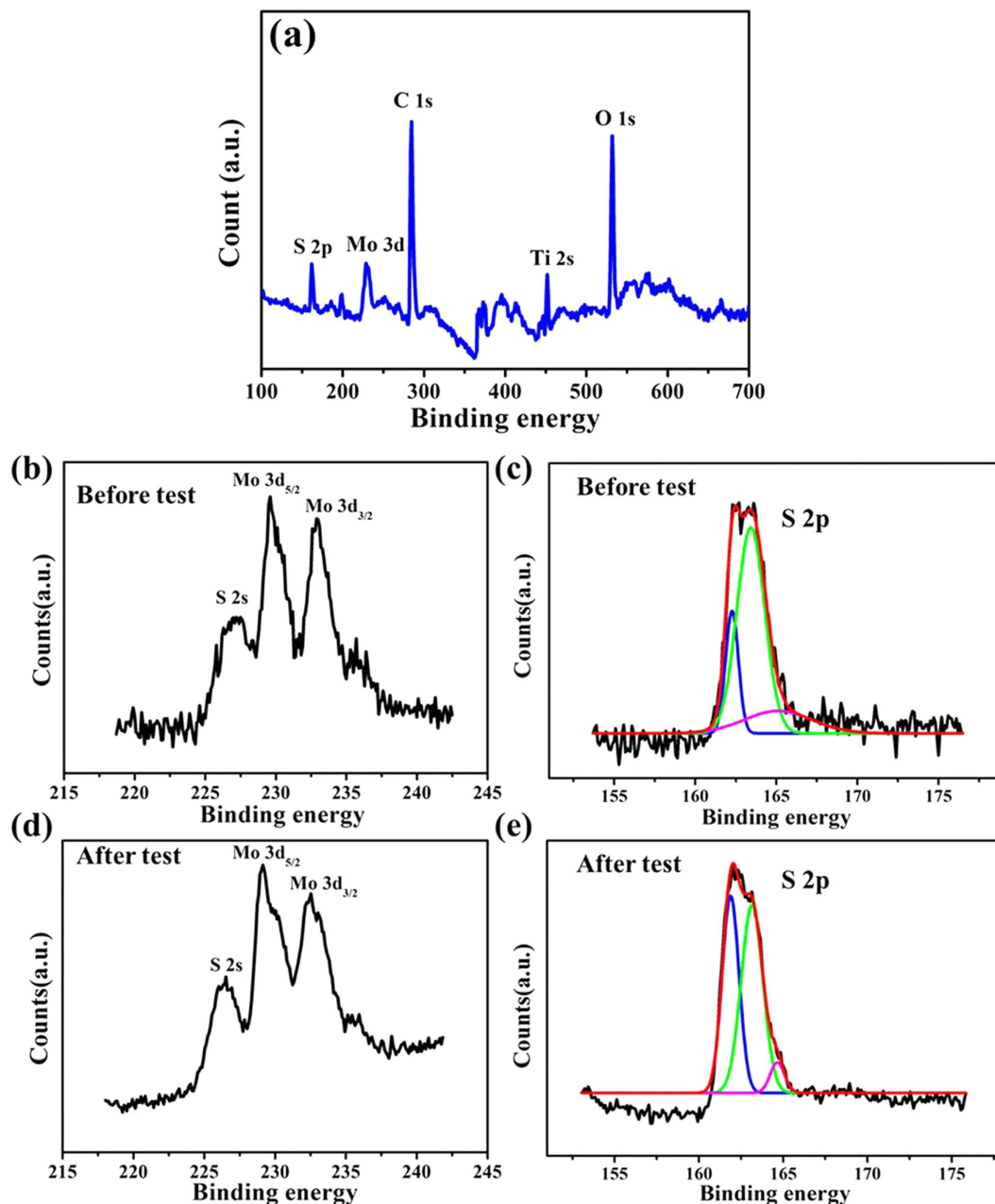
Figure 4. Chemical composition analyses. (**a**) XPS survey spectra. (**b,c**) XPS narrow spectra of Mo 3d and S 2p of as-synthesized MoS$_x$/Ti/InP electrode. (**d,e**) XPS narrow spectra of Mo 3d and S 2p of the MoS$_x$/Ti/InP electrode after 2 h PEC test at 0 V vs. RHE in a PEC scheme.

To study the PEC water splitting performance, the photocurrent density vs. potential (J–V) curves of the pristine InP, MoS$_x$/InP and MoS$_x$/Ti/InP photocathodes were measured in dark and under simulated sunlight illumination (100 mW cm^{-2}). All experiments were performed under the same conditions, using 1 M HClO$_4$ as electrolyte. The current densities were normalized with respect to the geometrical surface area and reported based on RHE scale. Figure 5a depicts the obtained best-performance J–V curves of the three InP-based photocathodes with optimized MoS$_x$ thickness. In dark, the current density is negligible. Under light illumination, the MoS$_x$/Ti/InP photocathode exhibits remarkable activity for PEC water reduction. The open-circuit voltage (V_{oc}) and the photocurrent at 0 V vs. RHE (J_{sc}) of the MoS$_x$/Ti/InP photocathode under illumination are 0.62 V vs RHE and 15.8 mA cm^{-2}, respectively, which both outperforms the pristine p-type InP, Ti/InP, and MoS$_x$/InP. To the best of our knowledge, the PEC performance of our MoS$_x$/Ti/InP is one of the best reported planar InP photocathodes decorated with noble-metal-free HER catalysts (Table S1). The largely enhanced PEC performance of the MoS$_x$/Ti/InP photocathode can be attributed to (i) an excellent electro-catalytic performance of MoS$_x$ which facilitates electron transfer to electrolyte for efficient proton reduction, and (ii) an enlarged band bending formed between Ti and p-InP due to the low work function of Ti (Fig. 1c). The resulting larger band bending favors
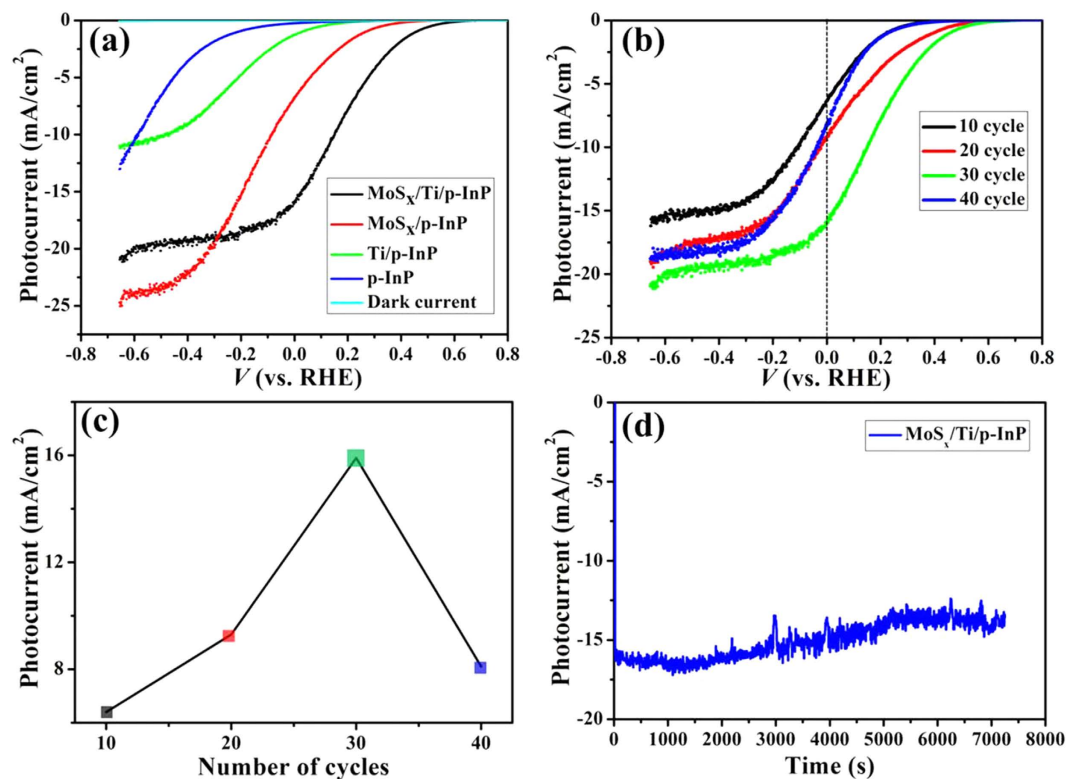
4

Figure 5. (**a**) Linear sweep voltammetry for pristine InP, MoS_x/InP and $MoS_x/Ti/InP$ photocathodes. (**b**) PEC Performances of the $MoS_x/Ti/InP$ photocathodes with different amount of MoS_x catalyst. (**c**) Comparison of j_{sc} at 0 V vs. RHE with different amount of MoS_x. (**d**) PEC stability measurements at 0 V vs. RHE with the best $MoS_x/Ti/InP$ photocathode.
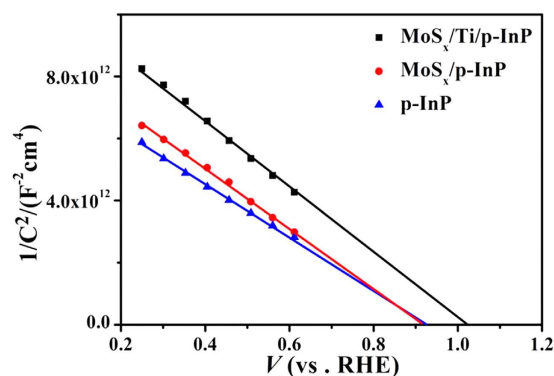

Figure 6. Mott-Schottky plots of pristine InP, MoS_x/InP and $MoS_x/Ti/InP$ photocathodes.

charge separation and charge transport. Therefore, $MoS_x/Ti/InP$ photocathode afforded a much more positive onset potential than the photocathode without the Ti layer. As shown in Fig. 5a, the PEC difference of InP with and without a Ti layer is clear. The increase of onset potential with Ti modified InP is in consistent with the positive shift of the flat-band potential of the same photocathode (Fig. 6). Moreover, it has been suggested that the Ti overlayer can protect InP from oxidation during the deposition process[26], which could be another contribution to the PEC improvement of Ti-coated InP photocathodes.

As discussed, a Ti layer on InP can effectively improve the performances, however, it reflects light to reduce light absorption in InP. As a result, the saturated photocurrent density with the $MoS_x/Ti/InP$ photocathodes is smaller than that of the MoS_x/InP without a Ti layer at relatively negative potentials (Fig. 5a). The achieved J_{sc} for $MoS_x/Ti/$ InP is still lower than that of the theoretically photocurrent density of 25–30 mA cm^{-2} for the InP photocathode[42]. Further improvement of the PEC performance is possible by improving light absorption using nanostructured InP photocathodes.

The PEC performance of $MoS_x/Ti/InP$ is determined by the amount of coated MoS_x, which is controlled by the number of CV cycles in the photoelectrodeposition experiments. A suitable amount of MoS_x on the top
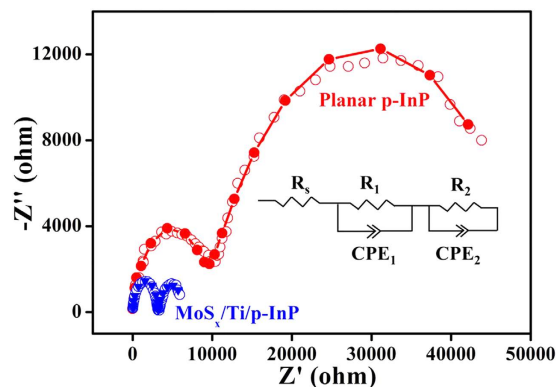
Figure 7. Nyquist plots of pristine InP and MoS$_x$/Ti/InP photocathodes. The scatter points in the plots represent the original experimental data, whereas the solid lines are the fitted curves using the equivalent circuit model in Fig. 7 (a).

surface is usually required to realize optimized PEC performances. We found that 20 and 30 cycles samples have better onset potential than 10 and 40 cycles samples as shown in Fig. 5b. The photocurrent density of MoS$_x$/Ti/InP loaded with different amount of MoS$_x$ measured at a potential of 0 V vs RHE is shown in Fig. 5c. MoS$_x$/Ti/InP with 30 CV cycles for MoS$_x$ deposition (corresponding to a ~32 nm a-MoS$_x$ layer with top-view and cross-section images shown in Fig. 3a,b), exhibit the best PEC performance. This is because there is a trade-off between the electro-catalytic activity and light flux. In other words, the electro-catalytic activity will increase with the amount of MoS$_x$[43]; whereas the light flux absorbed by MoS$_x$/Ti/InP will be decreased with the increase of MoS$_x$ amount. Therefore, there would be an optimal amount of MoS$_x$ for the best PEC performance.

The PEC stability of MoS$_x$/Ti/InP photocathodes was investigated at 0 V vs. RHE under continuous simulated solar light illumination (Fig. 5d). PEC photocurrent density remained almost stable over 2 h with only a small decrease from the initial value of 15.8 to ~14 mA cm^{-2} after a 2 h PEC test. The decay of photocurrent density is likely attributed to the degradation of the Ti layer[44] and/or the H$_2$ bubble generation during the stability test. Which is coincides with the visual observation of an excess amount of H$_2$ bubbles accumulating on the electrode surface; these bubbles block some active area and interfere with the diffusion of the electrolyte to the photocathode. Moreover, the fluctuation in the photocurrent density is closely related to the bubbling of hydrogen.

To investigate the electronic properties of the pristine and modified InP photocathodes in electrolyte, Mott-Schottky analyses were performed in dark. The flat band potential, V_{fb}, is determined from the interception of the plot of C^{-2} versus potential curve. The carrier concentration is calculated using the slope of the linear region according to the following equation:

$$\frac{1}{C^2} = \left(\frac{2}{e_0 \varepsilon \varepsilon_0 N_d A^2}\right)\left(V - V_{fb} - \frac{k_B T}{e_0}\right)$$

where C is the space charge capacitance, e_0 is the electron charge, ε and ε_o are the dielectric constant of the measured semiconductor and permittivity of the vacuum respectively, N_d is the carrier density, A is the measured electrode area, V is the applied potential, V_{fb} is the flat band potential of the measured semiconductor in electrolyte, k_B is the Boltzmann constant, and T is the absolute temperature.

Figure 6 shows that all InP samples have negative slopes in the Mott-Schottky plots, indicating that the samples are all p-type semiconductors. The carrier density of InP determined from the slope of the Mott-Schottky plot is ~1.1×10^{18} cm^{-3}, which agrees with the value from the InP wafer vendor. The V_{fb} of the pristine InP electrode is estimated to be ~0.92 V vs. RHE close to the previous report[21]. The V_{fb} for MoS$_x$/InP is almost the same as that of pristine InP, which is also in consistent with other reports[20,27]. However, the V_{fb} of MoS$_x$/Ti/InP electrode cathodically shifts from ~0.92 to ~1.02 V vs. RHE, indicating an increased surface band bending, because the low work function of Ti affords a high Schottky barrier to the p-type InP valence band[44,45]. The increased band bending (Fig. 1b) is advantageous to efficiently separate charges and facilitate charge transfer with a reduced recombination loss. Therefore, MoS$_x$/Ti/InP provides a much more positive onset potential for hydrogen evolution than the MoS$_x$/InP electrode as observed in Fig. 5a. This increase is comparable to a different work by enhancing the photovoltage generated by InP in aqueous solutions[21].

To gain more insight into the principle of the enhancement of PEC performance, electrochemical impedance spectroscopy (EIS) was conducted for different samples under simulated solar light illumination. The circle curves in Fig. 7 are experimental data and solid lines represent fitting results. An equivalent circuit is shown in Fig. 7. As indicated, the equivalent circuit model fitted well with both of the InP electrodes. Two semicircles can be clearly distinguished from Nyquist plots of each sample. The semicircle in the high frequency range is attributed to the depletion layer in semiconductor and the semicircle in the low frequency range is attributed to the capacitance at the semiconductor/electrolyte interface. In our model, R$_s$ represents the overall series resistance of the circuit, R$_1$ and CPE$_1$ correspond to the charge transfer resistance and the depletion layer capacitance in the semiconductor, R$_2$ and CPE$_2$ are associated with the charge transfer resistance and double layer capacitance at semiconductor/

Sample	R_S (Ω)	R_1 (Ω)	CPE_1 (nF)	R_2 (Ω)	CPE_2 (μF)
InP	4.37 ± 0.17	10670 ± 310	64.7 ± 5.23	47536 ± 2159	23.5 ± 1.23
MoS_x/Ti/InP	3.92 ± 0.11	3214 ± 20	25.3 ± 1.38	3013 ± 155	178.3 ± 9.31

Table 1. Resistances and capacitances determined from Nyquist plots.

electrolyte interface. Two constant phase elements (CPE) can be visualized as a non-ideal capacitor. It has been suggested that smaller arc radius in Nyquist plot implies a more effective charge separation of electron-hole pairs and a faster interfacial charge transfer[46]. Significantly, MoS_x/Ti/InP show much smaller semicircle, suggesting much smaller charge transfer resistance in MoS_x/Ti/InP, in comparison with the pristine InP electrode.

The fitted data of each element in the model are summarized in Table 1, among which some features deserve attention. The values of R_2 for MoS_x/Ti/InP and InP are 3013 ohm, 47536 ohm, respectively. The charge transfer resistance of double layer in MoS_x/Ti/InP sample is approximately 16 times smaller than that of pristine InP sample, showing a good correlation with the remarkably enhanced photocurrent density in MoS_x/Ti/InP photocathodes (Fig. 5a). MoS_x modification reduced the charge transfer resistance and increased the capacitance mainly at MoS_x/Ti/InP/electrolyte interface, i.e. the surface of the photocathode where water reduction reaction takes place. Therefore we can conclude that MoS_x loading promotes the charge separation and water reduction reaction on the InP surface. This is consistent with the reported results that MoS_x is an effective electrocatalyst for the hydrogen evolution reaction. In addition, MoS_x/Ti/InP photocathode leads to fast charge transfer in semiconductor bulk, which is attributed to the larger band bending in the photocathode. These results clearly explain the remarkably enhanced performance of the MoS_x/Ti/InP electrode.

In summary, a noble-metal-free MoS_x/Ti/InP photocathode was fabricated by simple deposition processes for solar hydrogen production. MoS_x/Ti/InP exhibited remarkably enhanced PEC performance in comparison with pristine p-InP and MoS_x/InP. Specifically, high photocurrent densities and relatively positive onset potentials were observed. The enhancement of PEC performance can be attributed to the excellent electro-catalytic activity of amorphous MoS_x nanomaterials, which reduces remarkably the charge transfer resistance at the semiconductor/electrolyte interface and increases the kinetics of water reduction. Moreover, the Ti buffer layer was a key component to realize a high photovoltage and to prevent the InP photocorrosion. The performance of MoS_x/Ti/InP was also dependent on the amount of surface MoS_x, for realizing optimal electro-catalytic activity on photocathode surfaces and absorption in InP. More importantly, the photocathodes were stable under continuous simulated solar light illumination over 2 h. Our simple and effective fabrication and surface modification processes are applicable to various photocathodes materials for enhancing their PEC performances.

Methods

Preparation of pristine InP samples. The wafers used in this work were one-side polished Zn-doped p-type (100)-oriented InP (MTI Corp.) with a carrier concentration of $\sim 10^{18}$ cm^{-3}. To fabricate InP working electrodes, wafers were cleaved into small pieces along the natural (110) cleavage planes. InP pieces were firstly degreased by successively sonicating in trichloroethylene, acetone and methanol for 5 min in each step to remove contaminants followed by washing in deionized water and then drying in N_2 flow. The pieces were then etched with HF (49%) and H_2O (1:10) for 1 min to remove the native oxides from surface. The InP wafers were then thoroughly rinsed using deionized water and dried under a flow of N_2.

Sputtering deposition of Ti layers. An ultrathin buffer layer of ~10 nm Ti film was deposited using Denton RF magnetron sputtering. Ti Target (99.95%) was pre-sputtered using RF power (300 W) at a high pressure of 10 mTorr to remove surface impurities prior to the deposition of Ti. The Ti layers were sputtered in an Ar environment. Until the chamber pressure reached 4×10^{-4} mTorr, sputtering was conducted. During sputtering, the working pressure inside the chamber was kept at 3.4 mTorr and the deposition power was kept at 200 W. Substrates were held at room temperature in all runs. Deposition rate at this condition was about 2.5 Å/s. InP was held at a room temperature during sputtering. Deposition rate at this condition was about 2.5 Å/s. The sputtered Ti layer protects InP photocathodes from aqueous solutions and transports photogenerated electrons to electrolyte when water reduction takes place.

Preparation of electrodes. ~60 nm thick Au was deposited on the back side of all InP samples using a thermal evaporator. An ohmic contact between Au and InP was formed. Then, high purity Ag pastes were used to attach Au on Cu plates. The copper plates were then covered with epoxy to ensure that only InP pieces were exposed to electrolyte. Copper plates with pieces were pressed in O-rings of electrochemical cells.

Preparation of MoS_x on InP electrodes. PEC deposition of MoS_x catalyst on InP and Ti/InP electrodes was performed under simulated 1 sun illumination. A freshly prepared photocathode was immersed into a 0.5 mM aqueous solution of $(NH_4)_2MoS_4$ in a 0.1 M phosphate buffer solution at pH 7. The MoS_x catalyst was deposited by continuous cyclic voltammograms performed using a Princeton potentiostat (PARSTAT 4000) with a saturated Ag/AgCl electrode as a reference electrode and a titanium wire as a counter electrode. The cyclic voltammograms were performed between 0 and +0.9 V vs. RHE at a scan rate of 0.05 Vs^{-1}. After this, we carefully washed the InP electrodes by dipping into deionized water several times to eliminate phosphate and $[MoS4]^{2-}$ ions.

Characterizations and PEC measurements. The sample morphologies were observed using a field-emission scanning electron microscope (FE-SEM, FEI Sirion 200). The surface composition of the sample

was analyzed by x-ray photoelectron spectroscopy (XPS, AXIS ULTRA DLD, Kratos, Japan). The binding energy was calibrated with the C1s level of 284.5 eV from surface contaminants. Water splitting performances of photoelectrodes were evaluated in a three-electrode PEC cell with an electrochemical workstation (PARSTAT 4000 model Princeton Applied Research fitted with an impedance analyzer). 1 M $HClO_4$ (pH = 0.5) solution was used as the electrolyte. InP, MoS_x/InP and MoS_x/Ti/InP photocathodes, a platinum (Pt) gauze, and a Ag/AgCl electrode were used as the working, counter, and reference electrodes, respectively. All three electrodes were put into a glass cell with a quartz window through which the working electrodes were illuminated from the front sides by a solar simulator (SOLARDGE 700, a 300 W xenon arc lamp equipped with an air mass (AM) 1.5 G filter). The incident light intensity was adjusted to 100 mW cm^{-2} by changing the position of lamp relative to that of the electrochemical cell. Before illumination, high-purity N_2 was purged into cells for 30 min. to remove the dissolved O_2. The PEC photocurrent density-voltage linear sweeping voltammetry (LSV) curves were measured under interrupted light illumination (100 mW cm^{-2}) sweeping form positive potentials to negative potentials with a scan rate of 10 mV s^{-1}. The PEC stability test was evaluated under light irradiation at a fixed potential of 0 V vs. RHE. The measured potentials vs. Ag/AgCl were converted to the reversible hydrogen electrode (RHE) according to the equation of $E_{RHE} = E_{Ag/AgCl} + 0.059 \, pH + E^0_{Ag/AgCl}$, where E_{RHE} is the converted potential vs. RHE, $E_{Ag/AgCl}$ is the experimental potential measured against the Ag/AgCl reference electrode, and $E^0_{Ag/AgCl}$ is the standard potential of Ag/AgCl at 25 °C (0.1976 V).

The Mott-Schottky and electrochemical impedance spectroscopy (EIS) measurements were performed using the same electrochemical measurement system for PEC measurements. Mott-Schottky measurements were obtained under dark conditions at a frequency of 1000 Hz in a 1 M $HClO_4$ solution with a scan rate of 10 mV/s. EIS data were collected under light (100 mW cm^{-2}) at +0.1 V vs RHE, with AC perturbation amplitude of 10 mV and a frequency within 10^5 to 10^{-1} Hz. The EIS spectra were fitted to an appropriate electrical analogue using ZView software.

References

1. Kudo, A. & Miseki, Y. Heterogeneous photocatalyst materials for water splitting. *Chem. Soc. Rev.* **38,** 253–278 (2009).
2. Kamat, P. V., Tvrdy, K., Baker, D. R. & Radich, J. G. Beyond photovoltaics: semiconductor nanoarchitectures for liquid-junction solar cells. *Chem. Rev.* **110,** 6664 (2010).
3. Osterloh, F. E. Inorganic nanostructures for photoelectrochemical and photocatalytic water splitting. *Chem. Soc. Rev.* **42,** 2294–2320 (2013).
4. Tachibana, Y., Vayssieres, L. & Durrant, J. R. Artificial photosynthesis for solar water-splitting. *Nat. Photonics* **6,** 511–518 (2012).
5. Zhang, T. & Lin, W. Metal-organic frameworks for artificial photosynthesis and photocatalysis. *Chem. Soc. Rev.* **43,** 5982–5993 (2014).
6. Walter, M. G. *et al.* Solar water splitting cells. *Chem. Rev.* **110,** 6446–6473 (2010).
7. Fujishima, A. & Honda, K. Electrochemical photolysis of water at a semiconductor electrode. *Nature* **238,** 37–38 (1972).
8. Paracchino, A. *et al.* Ultrathin films on copper(i) oxide water splitting photocathodes: a study on performance and stability. *Energ. Environ. Sci.* **5,** 8673 (2012).
9. Lin, Y. *et al.* Amorphous Si thin film based photocathodes with high photovoltage for efficient hydrogen production. *Nano lett.* **13,** 5615–5618 (2013).
10. Rovelli, L., Tilley, S. D. & Sivula, K. Optimization and stabilization of electrodeposited Cu_2ZnSnS_4 photocathodes for solar water reduction. *ACS Appl. Mat. Interfaces* **5,** 8018–8024 (2013).
11. Schreier, M. *et al.* Efficient and selective carbon dioxide reduction on low cost protected Cu_2O photocathodes using a molecular catalyst. *Energ. Environ. Sci.* **8,** 855–861 (2015).
12. Shaner, M. R., McKone, J. R., Gray, H. B. & Lewis, N. S. Functional integration of Ni–Mo electrocatalysts with Si microwire array photocathodes to simultaneously achieve high fill factors and light-limited photocurrent densities for solar-driven hydrogen evolution. *Energ. Environ. Sci.* **8,** 2977–2984 (2015).
13. Van de Krol, R., Liang, Y. & Schoonman, J. Solar hydrogen production with nanostructured metal oxides. *J. Mater. Chem.* **18,** 2311 (2008).
14. Khaselev, O. A Monolithic photovoltaic-photoelectrochemical device for hydrogen production via water splitting. *Science* **280,** 425–427 (1998).
15. Reece, S. Y. *et al.* Wireless solar water splitting using silicon-based semiconductors and earth-abundant catalysts. *Science* **334,** 645–648 (2011).
16. Lee, M. H. *et al.* p-Type InP nanopillar photocathodes for efficient solar-driven hydrogen production. *Angew. Chem. Int. Ed.* **51,** 10760–10764 (2012).
17. Heller, A. 11.5% solar conversion efficiency in the photocathodically protected p-InP/V^{3+}-V^{2+}-HCI/C semiconductor liquid junction cell. *Appl. Phys, Lett.* **38,** 282 (1981).
18. Heller, A. & Vadimsky, R. Efficient solar to chemical conversion: 12% efficient photoassisted electrolysis in the [p-type InP(Ru)]/HCl-KCl/Pt(Rh) cell. *Phys. Rev. Lett.* **46,** 1153–1156 (1981).
19. Ang, P. G. P. & Sammells, A. F. Hydrogen evolution at p-lnP photocathodes in alkaline electrolyte. *J. Electrochem. Soc* **131,** 1462–1464 (1984).
20. Gao, L. *et al.* Photoelectrochemical hydrogen production on InP nanowire arrays with molybdenum sulfide electrocatalysts. *Nano lett.* **14,** 3715–3719 (2014).
21. Gao, L. *et al.* High-efficiency InP-based photocathode for hydrogen production by interface energetics design and photon management. *Adv. Funct. Mater* **26,** 679–686 (2016).
22. Uosaki, K. & Kita, H. Photocathodic reactions at p-InP. *Solar Energy Mater.* **7,** 421–429 (1983).
23. Döscher, H. *et al.* Epitaxial III–V films and surfaces for photoelectrocatalysis. *Chemphyschem.* **13,** 2899–2909 (2012).
24. Hettick, M. *et al.* Nonepitaxial thin-film InP for scalable and efficient photocathodes. *J. Phys. Chem. Lett.* **6,** 2177–2182 (2015).
25. Lin, Y. *et al.* Role of TiO_2 surface passivation on improving the performance of p-InP photocathodes. *J. Phys. Chem. C* 150126152338001 (2015).
26. Seger, B. *et al.* Hydrogen production using a molybdenum sulfide catalyst on a titanium-protected n(+)p-silicon photocathode. *Angew. Chem. Int. Ed.* **51,** 9128–9131 (2012).
27. Huang, Z. *et al.* Enhanced photoelectrochemical hydrogen production using silicon nanowires@MoS_3. *Nano Energy* **2,** 1337–1346 (2013).
28. Benck, J. D. *et al.* Designing active and stable silicon photocathodes for solar hydrogen production using molybdenum sulfide nanomaterials. *Adv. Energy Mater.* **4,** 1400739–1400746 (2014).

29. Morales-Guio, C. G., Tilley, S. D., Vrubel, H., Gratzel, M. & Hu, X. Hydrogen evolution from a copper(I) oxide photocathode coated with an amorphous molybdenum sulphide catalyst. *Nat. Commun.* **5,** 3059 (2014).
30. Raja, R. *et al.* Pt-free solar driven photoelectrochemical hydrogen fuel generation using 1T MoS_2 co-catalyst assembled CdS QDs/TiO_2 photoelectrode. *Chem Commun* **51,** 522–525 (2015).
31. Boettcher, S. W. *et al.* Photoelectrochemical hydrogen evolution using Si microwire arrays. *J. Am. Chem. Soc.* **133,** 1216–1219 (2011).
32. Li, C. *et al.* Positive onset potential and stability of Cu_2O-based photocathodes in water splitting by atomic layer deposition of a Ga_2O_3 buffer layer. *Energ. Environ. Sci.* **8,** 1493–1500 (2015).
33. Merki, D., Fierro, S., Vrubel, H. & Hu, X. Amorphous molybdenum sulfide films as catalysts for electrochemical hydrogen production in water. *Chem. Sci.* **2,** 1262–1267 (2011).
34. Li, P. *et al.* Subnanometer molybdenum sulfide on carbon nanotubes as a highly active and stable electrocatalyst for hydrogen evolution reaction. *ACS Appl. Mater. Inter.* **8,** 3543–3550 (2016).
35. Lin, T.-W., Liu, C.-J. & Lin, J.-Y. Facile synthesis of MoS_3/carbon nanotube nanocomposite with high catalytic activity toward hydrogen evolution reaction. *Appl. Catal. B.* **134–135,** 75–82 (2013).
36. Vrubel, H., Merki, D. & Hu, X. Hydrogen evolution catalyzed by MoS_3 and MoS_2 particles. *Energ. Environ. Sci.* **5,** 6136 (2012).
37. Kibsgaard, J., Jaramillo, T. F. & Besenbacher, F. Building an appropriate active-site motif into a hydrogen-evolution catalyst with thiomolybdate $[Mo_3S_{13}]^{2-}$ clusters. *Nat. Chem.* **6,** 248–253 (2014).
38. Wang, H. W., Skeldon, P. & Thompson, G. E. XPS studies of MoS_2 formation from ammonium tetrathiomolybdate solutions *Surface and Coatings Technolog* **91,** 200–207 (1997).
39. Vrubel, H. & Hu, X. Growth and activation of an amorphous molybdenum sulfide hydrogen evolving catalyst. *ACS Catal.* **3,** 2002–2011 (2013).
40. Li, D. J. *et al.* Molybdenum sulfide/N-doped CNT forest hybrid catalysts for high-performance hydrogen evolution reaction. *Nano lett.* **14,** 1228–1233 (2014).
41. Zheng, Y., Jiao, Y., Jaroniec, M. & Qiao, S. Z. Advancing the electrochemistry of the hydrogen-evolution reaction through combining experiment and theory. *Angew. Chem. Int. Ed.* **54,** 52–65 (2015).
42. Kang, D. *et al.* Electrochemical synthesis of photoelectrodes and catalysts for use in solar water splitting. *Chem. Rev.* **115,** 12839–12887 (2015).
43. McAteer, D. *et al.* Thickness dependence and percolation scaling of hydrogen production rate in MoS_2 nanosheet and nanosheet-carbon nanotube composite catalytic electrodes. *ACS Nano* **10,** 672–683 (2016).
44. Feng, J. *et al.* Nickel-coated silicon photocathode for water splitting in alkaline electrolytes. *Nano Research* **8,** 1577–1583 (2015).
45. Kenney, M. J. *et al.* High-performance silicon photoanodes passivated with ultrathin nickel films for water oxidation. *Science* **342,** 836–840 (2013).
46. Bell, N. J. *et al.* Understanding the enhancement in photoelectrochemical properties of photocatalytically prepared TiO_2-reduced graphene oxide composite. *J. Phys. Chem. C* **115,** 6004–6009 (2011).

Acknowledgements

Author Contributions

Q.L. and M.J.Z. planned the project. Q.L. and L.M. carried out the experiments. M.Z., L.G.M., F.W. and W.S. contributed in material characterization and discussion. Q.L. wrote the manuscript. All authors reviewed the manuscript.

Additional Information

Supplementary information accompanies this paper at http://www.nature.com/srep

Competing financial interests: The authors declare no competing financial interests.

How to cite this article: Li, Q. *et al.* Engineering MoS_x/Ti/InP Hybrid Photocathode for Improved Solar Hydrogen Production. *Sci. Rep.* **6,** 29738; doi: 10.1038/srep29738 (2016).